AGU PUBLICATIONS

JGR

Journal of Geophysical Research: Oceans

RESEARCH ARTICLE

10.1002/2015JC011141

The characteristics and dynamics of wave-driven flow across a platform coral reef in the Red Sea

S. J. Lentz[1], J. H. Churchill[1], K. A. Davis[2], J. T. Farrar[1], J. Pineda[3], and V. Starczak[3]

[1]Physical Oceanography Department, Woods Hole Oceanographic Institution, Woods Hole, Massachusetts, USA, [2]Civil and Environmental Engineering, University of California, Irvine, California, USA, [3]Biology Department, Woods Hole Oceanographic Institution, Woods Hole, Massachusetts, USA

Key Points:
- Currents across a platform reef in the Red Sea are driven by surface gravity wave setup
- Bottom drag coefficients for the depth-average currents depend on water depth
- Analytic model for platform reefs reproduces observed cross-reef and along-reef currents

Correspondence to:
S. J. Lentz,
slentz@whoi.edu

Citation:
Lentz, S. J., J. H. Churchill, K. A. Davis, J. T. Farrar, J. Pineda, and V. Starczak (2016), The characteristics and dynamics of wave-driven flow across a platform coral reef in the Red Sea, *J. Geophys. Res. Oceans*, *121*, 1360–1376, doi:10.1002/2015JC011141.

Received 14 JUL 2015
Accepted 26 JAN 2016
Accepted article online 29 JAN 2016
Published online 16 FEB 2016

Abstract Current dynamics across a platform reef in the Red Sea near Jeddah, Saudi Arabia, are examined using 18 months of current profile, pressure, surface wave, and wind observations. The platform reef is 700 m long, 200 m across with spatial and temporal variations in water depth over the reef ranging from 0.6 to 1.6 m. Surface waves breaking at the seaward edge of the reef cause a 2–10 cm setup of sea level that drives cross-reef currents of 5–20 cm s^{-1}. Bottom stress is a significant component of the wave setup balance in the surf zone. Over the reef flat, where waves are not breaking, the cross-reef pressure gradient associated with wave setup is balanced by bottom stress. The quadratic drag coefficient for the depth-average flow decreases with increasing water depth from $C_{da} = 0.17$ in 0.4 m of water to $C_{da} = 0.03$ in 1.2 m of water. The observed dependence of the drag coefficient on water depth is consistent with open-channel flow theory and a hydrodynamic roughness of $z_o = 0.06$ m. A simple one-dimensional model driven by incident surface waves and wind stress accurately reproduces the observed depth-averaged cross-reef currents and a portion of the weaker along-reef currents over the focus reef and two other Red Sea platform reefs. The model indicates the cross-reef current is wave forced and the along-reef current is partially wind forced.

1. Introduction

Shallow platform reefs are a prevalent feature throughout the Red Sea. However, there have been few studies of the current dynamics of Red Sea coral reefs, with the notable exception of the Gulf of Aqaba at the northern end of the Red Sea [*Monismith et al.*, 2006; *Reidenbach et al.*, 2006]. Flow across coral reefs is a key factor determining the exchange of water and constituents between reefs and the surrounding ocean, the residence time of water on the reef, and exchange between seawater and the coral bed. These physical factors, in turn, influence a variety of physical and biogeochemical processes that impact coral reef ecosystems such as the supply and uptake of nutrients [e.g., *Baird et al.*, 2004; *Falter et al.*, 2004; *Cuet et al.*, 2011] and the thermal environment [e.g., *Davis et al.*, 2011; *Oliver and Palumbi*, 2011; *Pineda et al.*, 2013].

Previous studies have shown that flows over many shallow coral reefs are driven by surface gravity waves [*Munk and Sargent*, 1948; *Von Arx*, 1954; *Roberts et al.*, 1975; *Symonds et al.*, 1995; *Kraines et al.*, 1998; *Callaghan et al.*, 2006; *Coronado et al.*, 2007; *Jago et al.*, 2007; *Hench et al.*, 2008; *Lowe et al.*, 2009; *Vetter et al.*, 2010; *Taebi et al.*, 2011; *Monismith et al.*, 2013]. The qualitative picture is well established; wave breaking at the front edge of the reef causes a setup of sea level and the resulting pressure gradient drives flow across the reef [*Munk and Sargent*, 1948; *Monismith*, 2007; *Hearn*, 2010]. Models of this process differ primarily in the character of the reef geometry and wave forcing [e.g., *Tait*, 1972; *Gourlay*, 1996a, 1996b; *Hearn*, 1999; *Massel and Gourlay*, 2000; *Gourlay and Colleter*, 2005] and in the parameterization of bottom stress [*Nelson*, 1996; *Nunes and Pawlak*, 2008; *Rosman and Hench*, 2011; *Jaramillo and Pawlak*, 2011; *Hearn*, 2011]. However, there have been few quantitative tests of these models. As noted by *Monismith* [2007], a key limitation to progress in quantifying wave-driven flow dynamics over coral reefs is the lack of simultaneous observations of sea level, currents, and waves to test models. In contrast to most of the previous observational studies of either barrier reefs or fringing reefs with a lagoon, this study focuses on an isolated platform reef. Isolated platform reefs provide a simpler system for investigating the wave-driven flow dynamics because they lack the dynamical complications of a coastal barrier or a fringing reef and lagoon system.

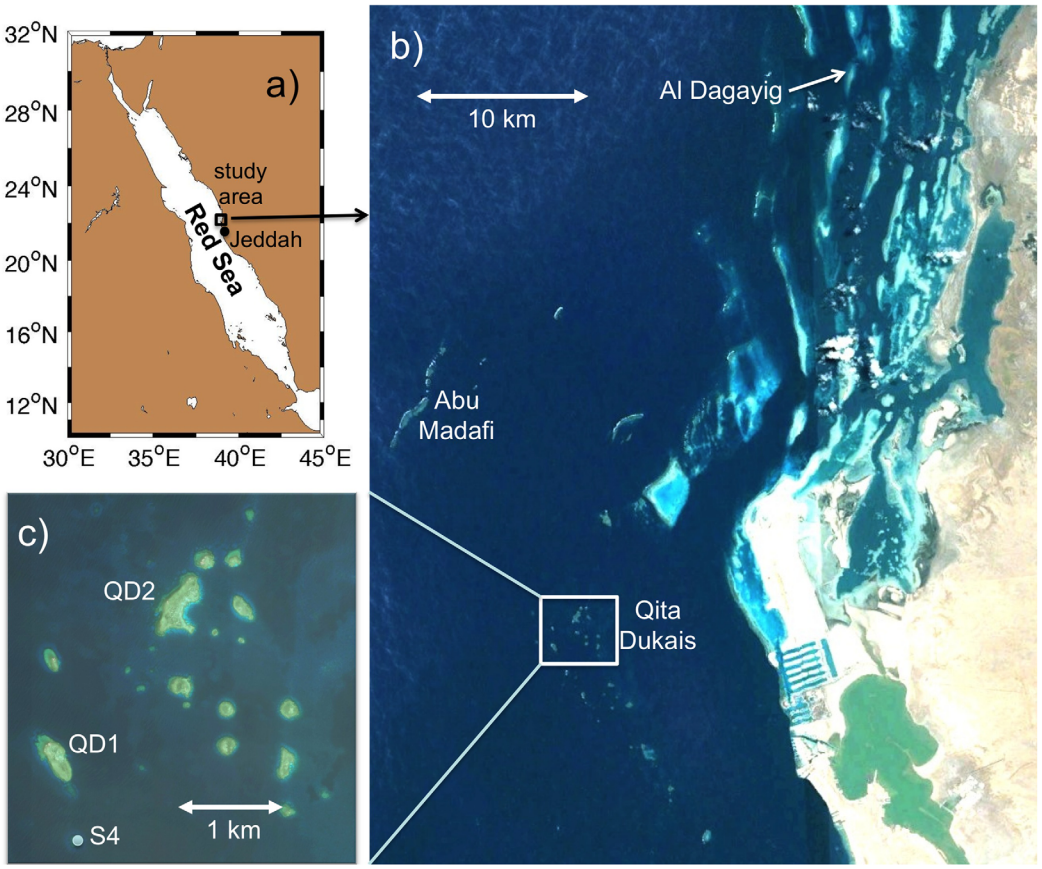

Figure 1. Satellite image (Google Earth) showing coral reefs along the eastern continental shelf of (b) the Red Sea, (a) north of Jeddah, Saudi Arabia. The focus of this study is a small reef, QD2, in (c) the Qita Dukais reef system (Apple Maps). Observations from QD1 in the Qita Dukais system, Al Dagayig to the north, and Abu Madafi at the shelf edge are also examined. Wave measurements were collected at site (c) S4 south of QD1.

The dynamics of the flow across a shallow platform coral reef in the Red Sea near Jeddah, Saudi Arabia (Figure 1), are studied using observations of currents, pressure, surface gravity waves, and wind (section 2). The dominant terms in the depth-averaged momentum balances are examined both in the surf zone at the front edge of the reef and the reef flat behind the surf zone where waves are not breaking (section 4). In contrast to most previous observational studies, a one-dimensional model of wave-driven flow across reefs (section 3) is used to interpret the observations and accurately account for the influence on the dynamics of cross-reef variations in water depth. A critical new element of this analysis is inclusion and evaluation of an open-channel flow model for the bottom drag coefficient for the depth-averaged current (section 3.2). The key feature of this model is that the drag coefficient depends on water depth, as well as bottom roughness. Over shallow coral reefs where there are substantial variations in water depth, this dependence of the drag coefficient on water depth may be critical both for accurately modeling the currents and for properly estimating hydrodynamic roughness. Finally, an analytic model for estimating currents over flat platform reefs, given incident wave characteristics, wind stress, water depth variations, hydrodynamic roughness, and the reef width, is proposed and tested using observations from three different reefs in the Red Sea (section 4.5).

2. Field Program and Processing

2.1. Field Site Description

This study focuses on the current dynamics across a platform reef (QD2, our designation) in the Qita Dukais reef system on the eastern side of the Red Sea approximately 50 km northwest of Jeddah, Saudi Arabia (Figure 1). QD2 is about 700 m long and 200 m across (Figure 2). The water depth relative to mean sea level

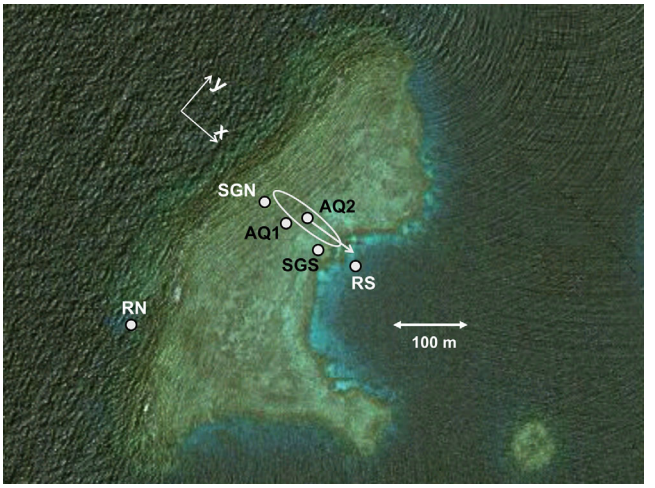

Figure 2. Satellite image (Apple Maps) of QD2 showing current profiler and pressure gauge locations. The depth-average mean current vector (magnitude 6 cm s^{-1}) and principal axes ellipse (major axis standard deviation 9 cm s^{-1}) for the AQ2 current profiler site are also shown. Mean depth-average current and principal axes ellipse are similar for AQ1. A right-handed coordinate system is adopted with *x* positive across the reef aligned with SGN and SGS.

varies across the reef platform from 0.6 m near the front (northwest side of the reef) to 1.2 m near the back (southeast side; Figure 3a). The back third of the reef contains sand channels that are 0.2–0.4 m deep (relative to the surrounding seafloor), 1–2 m wide, and several meters long (Figure 3a and light colored regions in Figure 2). At the edge of the reef, there is an abrupt drop, over a horizontal distance of 1–10 m, to depths of about 15 m in the surrounding water (Figure 3b).

2.2. Instrumentation, Locations, and Timing

Instruments were deployed across QD2 (Figures 2 and 3) for three consecutive 6 month periods: mid-November 2009 through May 2010, June through November 2010, and December 2010 through May 2011. This study focuses on observations from a midreef current profiler (AQ1 and AQ2 sites) bracketed by a pair of pressure gauges near the front (SGN) and back (SGS) edges of the reef.

During the first two study periods, a Nortek 2 MHz Aquadopp current profiler was deployed at AQ1, in a 2 m wide sand channel, about 130 m from the front edge of the reef. The current profiler site was shifted to AQ2 for the third deployment. AQ2 is slightly off the line between SGN and SGS, but is in a shallower region with more uniform water depths characteristic of the middle of the reef flat. Current observations are only available for the first half of the third deployment (prior to 6 March 2011) because a piece of coral rubble partially covered one of the acoustic heads. The Aquadopp was in pulse-coherent mode [e.g., *Zedel et al.*, 1996; *Veron and Melville*, 1999] sampling at 1 Hz for 256 s bursts every hour during all three deployments. The Aquadopp sampled current profiles in 14 bins, each with a vertical extent of 0.025 m, ranging from 0.41 mab (meters above the bottom) to 0.74 mab during the first two deployments and from 0.19 to 0.52 mab during the third deployment. The estimated accuracy of the mean current over each 256 s burst is ~3 mm s^{-1} [*Zedel et al.*, 1996; *Veron and Melville*, 1999].

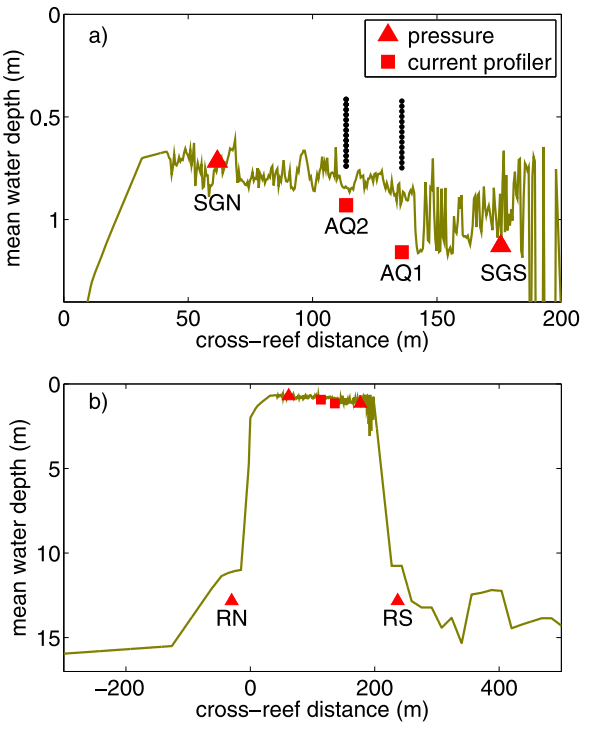

Figure 3. Bathymetry relative to mean sea level (a) along the QD2 across-reef instrument transect (Figure 2) and (b) over a broader transect encompassing the platform reef. Instrument locations and heights of current profiler bins are also shown.

Pressure was measured using Seabird Seagauges deployed 55 m from the front edge of the reef at SGN, and 10 m from the back edge of the reef at SGS (Figures 2 and 3a). Seagauges were also deployed on bottom tripods in 12 m of water in front of the reef at RN and behind the reef at RS during the first two deployments. All Seagauges

sampled pressure continuously, recording 10 min averages. To estimate significant wave height and peak wave period, the Seagauges at all sites except RN, sampled at 2 Hz for 512 s bursts every 4 h (for details on surface wave measurements and processing, see *Lentz et al.* [2016]). Seagauges were outfitted with parallel plate ports to reduce pressure perturbations associated with the flow impinging on the pressure port (Bernoulli effects). Previous studies and results presented here suggest that the pressure measurements have an accuracy of a few millimeters of water [*Lentz et al.*, 1999].

An RDI 1200 kHz Acoustic Doppler Current Profiler (ADCP) was also deployed on a bottom tripod at RN to measure surface waves and current profiles (Figures 2 and 3b). The ADCP collected 10 min burst samples at 2 Hz every 4 h to characterize surface waves. RDI WaveMon software was used to estimate significant wave height, peak wave period, and wave direction.

Wind and wave measurements were collected at a meteorological buoy in the Red Sea basin approximately 40 km northwest of Qita Dukais from mid-October 2008 to early December 2010 [*Jiang et al.*, 2009]. Wind measurements were also collected at a coastal tower located on the King Abdullah University of Sciences and Technology (KAUST) campus about 40 km northeast of Qita Dukais from mid-October 2008 to May 2011. Tower wind measurements are used after early December 2010 when the buoy wind measurements were no longer collected. Wind stresses, estimated using a bulk formula [*Fairall et al.*, 2003], include both a strong sea breeze and subtidal variability [*Jiang et al.*, 2009]. For the subtidal wind stresses of interest here, correlations between the two sites are 0.76 for the east-west component and 0.88 for the north-south component.

In addition to the QD2 observations, current profiles from Aquadopps deployed on two other reefs, QD1 (Figure 1c) and Al Dagayig (Figure 1b), are used in section 4.5 to test the model outlined in section 3. Pressure and wave measurements from two Seagauges deployed on Abu Madafi reef at the continental shelf edge (Figure 1b) are used to examine the wave setup balance (section 4.4). See Appendix A for descriptions of the QD1, Al Dagayig, and Abu Madafi reefs and measurements.

2.3. Processing

Initial processing and quality control of the data are described in Appendix B. All time series observations were placed on a common time base of hourly values. Currents and wind stresses were rotated into a right-handed coordinate system with the x axis oriented across-reef along the line between the SGN and SGS pressure gauges with x positive toward the back of the reef (140°T), and the y axis oriented along-reef (Figure 2). Depth-averaged flow was estimated using an empirical-orthogonal-function (EOF) analysis of the current profile time series and extrapolating the dominant mode to the surface and bottom (see section 4.2).

3. Model Framework

To interpret the observations and investigate the current dynamics over the reef, two simple models are combined. First, following *Symonds et al.* [1995], *Hearn* [1999], *Gourlay and Colleter* [2005], and others, a steady one-dimensional depth-averaged model for wave-driven and wind-driven flow across a platform reef is used to provide an explicit relationship between depth-average currents at a point, the bottom stress integrated across the reef, and the pressure difference across the reef. Second, a model of the velocity profile in rough-bottom open-channel flow is used to estimate of the bottom drag coefficient for depth-averaged flow in terms of a hydrodynamic roughness (z_o) and water depth [e.g., *Nezu and Nakagawa*, 1993].

3.1. Model for Depth-Average Flow Across a Platform Reef

Assuming steady state ($\partial/\partial t$ small compared to other terms) and no along-reef variations ($\partial/\partial y=0$), continuity implies that the cross-reef transport $q_o(t)$ does not vary across the reef:

$$U(\eta+\eta_o+h)=U(\eta+D)=q_o, \tag{1}$$

where $U(x, t)$ is the depth-averaged (Lagrangian) cross-reef current including the Stokes velocity due to waves [e.g., *Monismith*, 2007]. (The Stokes velocity is estimated to be a few mm s^{-1}, both in front of the reef at RN and over the reef flat.) $\eta(x, t)$ is the sea level variation over the scale of the reef due to wave forcing

(wave setup), $\eta_o(t)$ is the sea level variation on spatial scales that are large compared to the reef, which includes tides, wind forcing, and seasonal buoyancy forcing, $h(x)$ is the water depth relative to mean sea level when currents are weak and $D(x, t) = \eta_o(t) + h(x)$. The assumption of no along-reef variations is reasonable for an elongated straight reef (length $\gg$ width), without substantial along-reef variations in bathymetry, and where waves break uniformly along the length of the reef. We lack data to test this assumption, but visual observations of wave breaking at the site suggest it is reasonable (note waves in Figure 2). We also assume $\eta \ll D$, so that $\eta + D \approx D$ which is a reasonable assumption for the reefs considered here, where variations in η are typically centimeters and D is about 1 m.

The steady, depth-averaged cross-reef momentum balance is

$$\frac{\partial(U^2D)}{\partial x} = -gD\frac{\partial \eta}{\partial x} - \frac{1}{\rho}\frac{\partial S_{xx}}{\partial x} + \frac{\tau^{sx}}{\rho} - \frac{\tau^{bx}}{\rho}, \tag{2}$$

where $g = 9.8$ m s^{-2} is gravitational acceleration, ρ is density, S_{xx} is the cross-reef component of the wave-radiation stress tensor, τ^{sx} is the wind stress, and τ^{bx} is the bottom stress [e.g., *Mei*, 1983; *Lowe et al*., 2009]. Wave-radiation stress is estimated as

$$S_{xx} = \frac{\rho g H_s^2}{16}\left\{\left(\cos^2(\theta_w)+1\right)\frac{c_g}{c} - \frac{1}{2}\right\}, \tag{3}$$

where H_s is significant wave height, θ_w is wave direction, c_g is group velocity, and c is phase velocity [*Longuet-Higgins and Stewart*, 1962, 1964]. Direct estimates of the temporal acceleration, Coriolis, and buoyancy gradient terms neglected in (2) are two orders of magnitude smaller than the observed pressure gradient. The buoyancy term is small despite large temperature gradients across the reef [*Davis et al*., 2011] because the reef is so shallow.

Estimating bottom stress as

$$\tau^{bx} = \rho C_{da} U|U| = \rho C_{da}\frac{q_o|q_o|}{D^2}, \tag{4}$$

where $C_{da}(x, t)$ is a bulk drag coefficient for the depth-average current [e.g., *Rosman and Hench*, 2011], dividing (2) by D and using (1) yields

$$-\frac{q_o^2}{D^3}\frac{\partial D}{\partial x} = -g\frac{\partial \eta}{\partial x} - \frac{1}{\rho D}\frac{\partial S_{xx}}{\partial x} + \frac{\tau^{sx}}{\rho D} - C_{da}\frac{q_o|q_o|}{D^3}. \tag{5}$$

Integrating (5) from x_1 to x to estimate the sea level difference $\Delta\eta = \eta(x) - \eta(x_1)$:

$$g\Delta\eta = -q_o|q_o|\left(\int_{x_1}^{x} C_{da}D^{-3}dx + \frac{1}{2}sgn(q_o)D^{-2}\Big|_{x_1}^{x}\right) + \int_{x_1}^{x}\left(-\frac{1}{\rho D}\frac{\partial S_{xx}}{\partial x} + \frac{\tau^{sx}}{\rho D}\right)dx. \tag{6}$$

For an isolated platform reef, such as QD2, the transport q_o can be determined by noting that sea level is the same just in front of and behind the reef, that is $\eta(x_f) = \eta(x_b)$. This follows from noting that the pressure gradient along a path going around the reef must be balanced by either the nonlinear advective momentum flux (flow separation; $\Delta\eta \approx U_s^2/2g$) or bottom drag ($\Delta\eta \approx C_d U_s^2 L/(gD_s)$), where $U_s \approx 0.1$ m s^{-1} is the shelf current, $C_d \approx 0.1$ or less, $L \approx 1$ km is distance around the reef, and $D_s \approx 10$ m is the shelf water depth. In either case, the sea level difference between the front and back of the reef is 1 cm or less. This is consistent with the observed sea level difference between RN and RS, which is typically less than 1 cm. Evaluating (6) from x_f to x_b, setting $\Delta\eta = 0$, and solving for q_o yields

$$q_o|q_o| = \int_{x_f}^{x_b}\left(-\frac{1}{\rho D}\frac{\partial S_{xx}}{\partial x} + \frac{\tau^{sx}}{\rho D}\right)dx \Bigg/ \left(\int_{x_f}^{x_b} C_{da}D^{-3}dx + \frac{1}{2}sgn(q_o)D^{-2}\Big|_{x_f}^{x_b}\right). \tag{7}$$

The transport $q_o(t)$ and depth-average flow $U(x, t)$ can be estimated from (7) and (1) given the forcing $S_{xx}(x, t)$ and $\tau^{sx}(t)$, the water depth $D(x, t)$, and $C_{da}(x, t)$ (see below). The sea level variation across the reef $\eta(x, t)$ can then be estimated from (6). It is convenient to define a weighted bulk drag coefficient across a section of the reef as

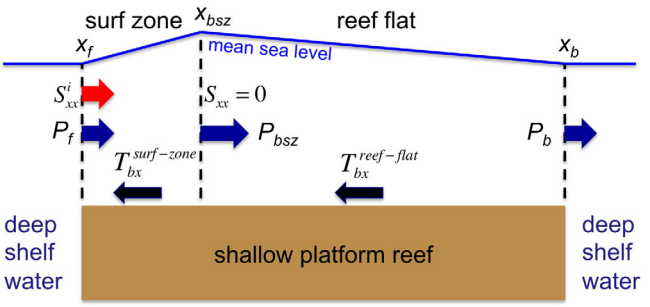

Figure 4. Schematic of force balances for the surf zone (x_f to x_{bsz}, region of wave breaking) and reef flat (x_{bsz} to x_b, no wave breaking) sections for the constant depth platform reef model, equation (9) section 3.1. S_{xx} is the momentum flux due to waves (radiation stress), P is the pressure force, and T_{bx} is the integrated bottom stress.

$$C_B(x,t)=\int_{x_1}^{x} C_{da}D^{-3}dx \Big/ \int_{x_1}^{x} D^{-3}dx. \tag{8}$$

Equation (7) can be further simplified for relatively flat platform reefs with an abrupt depth change to the surrounding shelf such as QD2 (e.g., Figure 3b, see also Figure 4). In this case, wave breaking and the resulting wave-radiation stress convergence must occur over the shallow reef flat after the abrupt change in bathymetry. Consequently, at the seaward edge of the shallow reef flat there has been no wave breaking and hence no wave-driven setup, so sea level is the same as in the deeper water just seaward of the abrupt change in bathymetry. (There is a slight "static" decrease in the sea level due to the wave shoaling. When the waves shoal the wave height should increase and there would be a slight increase in the set-down under the waves. This set-down is small and since it is a local Bernoulli balance between the wave kinetic energy and the sea level it has no impact on the reef current dynamics.) Wave reflection would slightly alter the wave-momentum flux onto the reef, but there is no discernible evidence of wave reflection in the directional spectrum from the ADCP just offshore of the reef [*Lentz et al.*, 2016]. Assuming water depth is independent of x over the reef flat, $D(x,t) \sim D(t)$, and the wave-radiation stress is small at the back of the reef relative to the front, $S_{xx}(x_f)-S_{xx}(x_b) \approx S_{xx}(x_f)$, (7) reduces to

$$U|U| \approx \frac{\left(-S^i_{xx}/\Delta x+\tau^{sx}\right)}{\rho C_{da}} \;\rightarrow\; U \approx sgn\left(-S^i_{xx}/\Delta x+\tau^{sx}\right)\sqrt{\frac{\left|-S^i_{xx}/\Delta x+\tau^{sx}\right|}{\rho C_{da}}}, \tag{9}$$

where S^i_{xx} is the incident wave-radiation stress and $\Delta x = x_b - x_f$. Equation (9) states that for a two-dimensional control volume over the reef, the on-reef flux of momentum due to the incident waves and the wind stress are balanced by the bottom stress.

To understand (9) consider the steady, depth-averaged force balance over a constant depth, one-dimensional platform reef divided into two sections, the first section extending from the front edge of the reef (x_f) to the back of the surf zone (x_{bsz}) and the second section extending from the back of the surf zone to the back of the reef (x_b; Figure 4). For simplicity assume no wind stress. The advective momentum flux is constant across the reef, and hence does not contribute to the force balance, because cross-reef transport and water depth are both constant across the reef. Consequently, the net forces on the surf zone section are the on-reef flux of momentum due to the waves, the pressures at each end of the section and the drag along the bottom (integrated bottom stress), i.e., $S^i_{xx}=(P_{bsz}-P_f)-T_{bx}^{surf-zone}$. For the reef flat section, the forces are just the pressures at each end of the section and the drag along the bottom, i.e., $0=(P_b-P_{bsz})-T_{bx}^{reef-flat}$. Summing the two sections to get the forces on the combined sections and noting that $P_f=P_b$ yields $S^i_{xx}=-T_{bx}^{surf-zone}-T_{bx}^{reef-flat}$. In other words, if the pressure and the advective momentum flux at the front and back of the reef are the same, the only net forces on the reef are the on-reef flux of momentum from the waves and the bottom stress.

The along-reef depth-average current V can be estimated from the along-reef depth-average momentum balance. Assuming the wave forcing is aligned with the x axis, no along-reef variations $(\partial/\partial y=0)$, $U \gg V$ so $\tau^{by} \approx \rho C_{da} V|U|$, and using $\partial q_o/\partial x=0$, the along-reef depth-average momentum balance (similar to equation (2)) reduces to

$$\frac{\partial(UVD)}{\partial x}=q_o\frac{\partial V}{\partial x}=\frac{\tau^{sy}}{\rho}-C_{da}V\frac{|q_o|}{D}. \tag{10}$$

Equation (10) can be integrated in x, but to reduce (10) to the simplest possible case, assume the cross-reef length scales are large compared to D/C_{da} so that $q_o\partial V/\partial x$ is small compared to the bottom stress. In this case:

$$V \approx \frac{\tau^{sy}}{\rho C_{da}}|U|. \tag{11}$$

Equations (9) and (11) are tested in section 4.5 using observations from three Red Sea platform reefs.

3.2. Open-Channel Flow Model of C_{da}

An estimate of C_{da} is needed to close the model outlined above. Assuming open-channel flow, the current profile is well represented by

$$u(\tilde{z}) = \frac{u_*}{\kappa}\left\{\log\left(\frac{\tilde{z}}{z_o}\right) + 2\Pi \sin^2\left(\frac{\pi\tilde{z}}{2D}\right)\right\}, \tag{12}$$

where $u(\tilde{z})$ is the velocity profile, $\kappa = 0.4$ is the von Karman constant, u_* is the shear velocity, $\tilde{z}$ is height above the bottom, z_o is the hydrodynamic roughness, and Π is Cole's wake strength [e.g., *Nezu and Nakagawa*, 1993, see also *Rosman and Hench*, 2011]. The first term on the right-hand side of (12) is the classic law-of-the-wall logarithmic profile and the second term is Cole's wake function that accounts for the vertically uniform pressure gradient driving the flow.

Integrating (12) from $\tilde{z} = z_o$ to $\tilde{z} = D$ and assuming $z_o \ll D$ the transport is

$$q \approx \frac{Du_*}{\kappa}\left[\log\left(\frac{D}{z_o}\right) + (\Pi - 1)\right]. \tag{13}$$

Using (4) and noting that $\rho u_*^2 = |\tau^b|$ yields [e.g., *Schlichting*, 1968; *Nezu and Nakagawa*, 1993]

$$C_{da} \approx \kappa^2\left\{\log\left(\frac{D}{z_o}\right) + (\Pi - 1)\right\}^{-2} \tag{14}$$

The key result is that $C_{da}(x, t)$ depends on the water depth $D(x, t)$, as well as z_o and Π. For high Reynolds number open-channel flow $\Pi \approx 0.2$ [*Nezu and Nakagawa*, 1993, Figure 4.2, see also *Rosman and Hench*, 2011 for application to coral reefs] and this value is used here. However, the choice of Π influences the estimation of z_o since $\Pi - \log(z_o)$ is a constant in (14).

The expression for the drag coefficient (14) does not account for the influence of surface gravity waves, which may increase the bottom stress and the apparent drag coefficient for currents [e.g., *Grant and Madsen*, 1982]. The influence of surface waves on bottom stress is briefly discussed in section 5.3 (see also sections 4.3 and 4.4).

4. Results

4.1. Overview of Wind Stress, Surface Waves, Currents, and Sea Level Characteristics

Wind stresses are primarily southeastward, along the axis of the Red Sea with peak magnitudes of about 0.3 N m^{-2} (Figure 5a) [*Sofianos and Johns*, 2003]. There are a few northward and westward wind events in winter. Diurnal winds (sea breeze) are stronger near the coast, but are still substantial at the meteorological buoy in the Red Sea basin [*Jiang et al*., 2009].

Significant wave heights at RN, in front of QD2, occasionally exceed 1 m (Figure 5b) with peak periods of 4–8 s and waves are generally from the north to northwest (−65°N to 25°N 87% of the time for $H_s^{RN} > 0.1$ m). Significant wave heights at RN are correlated ($r = 0.89$) with significant wave heights at the meteorological buoy in the Red Sea basin but are about half the amplitude [*Lentz et al*., 2016]. Waves typically break at the front edge of the reef so that wave heights are less than 0.3 m on top of the reef, at SGN and SGS (Figure 5b). See *Lentz et al*. [2016] for a detailed description of the wave transformation across QD2.

Depth-averaged currents over QD2 are polarized in the cross-reef direction (Figure 2, ellipse) with southeastward flow events of 0.1–0.2 m s^{-1} that persist for days (Figure 5c, blue trace) and are clearly related to the wave heights and the wind stresses (correlations 0.83 and 0.70, respectively). A water parcel crosses the 200 m wide reef in 15–30 min during these current events. Along-reef currents are relatively small, typically a few cm s^{-1} (Figure 5c, red trace).

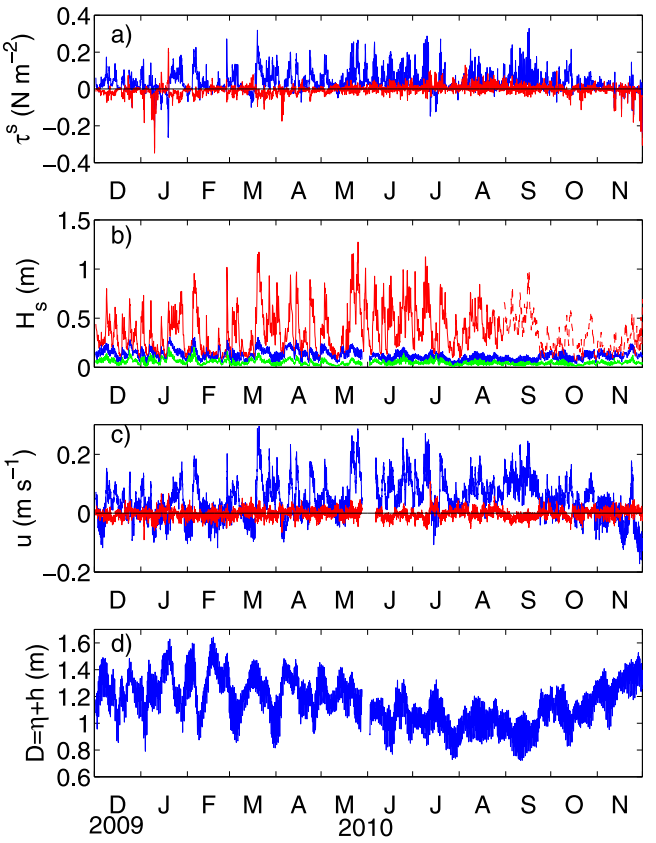

Figure 5. Time series of (a) southeastward (blue) and southwestward (red) wind stress, (b) significant wave heights at RN (red), SGN (blue), and SGS (green) over QD2, (c) depth-average cross-reef (blue) and along-reef (red) currents at AQ1, and (d) water depth at AQ1. The dashed red line in Figure 5b indicates wave heights inferred from offshore sites when wave heights at RN were not available.

Temporal variations in water depth at AQ1 range from 0.8 to 1.6 m (Figure 5d) and are associated with large-scale sea level variations $\eta_o(t)$ at annual, synoptic (days), and tidal time scales. The amplitude of the annual variation is 0.15 m with a maximum in winter (January–February) and minimum in summer (July–September), consistent with previous observations of sea level variations in the Red Sea [*Morcos*, 1970; *Osman*, 1985; *Sultan et al*., 1995; *Abdelrahman*, 1997; *Manasrah et al*., 2009]. Synoptic and tidal variability have standard deviations of 0.10 and 0.07 m, respectively. Synoptic variations are larger in winter than in summer, with water depth variations of as much as 0.5 m over time scales of a few days, e.g., early February 2010 (Figure 5d).

4.2. Vertical Structure of the Reef Flat Currents

Current profiles at sites AQ1 and AQ2 on QD2 have a remarkably consistent vertical structure. A single vertical structure with time-varying amplitude, associated with the dominant empirical-orthogonal-function (EOF) mode, accounts for 99.2%, 99.3%, and 98.8% of the total current variance during the three deployments. The large fraction of variance accounted for by the dominant mode indicates that the current amplitude varies in time but to first order the vertical structure of the currents does not, that is $u(t,z)=A(t)Z(z)$ where A is the time-varying amplitude and Z is the vertical structure. The dominant EOF current profile is unidirectional and is a logarithmic function of height above the bottom (Figure 6). There is a slight deviation from a logarithmic profile near the bottom of each profile that is probably due to deflection of the flow around the instrument housing and mounting frame. A rough estimate of the flow distortion based on potential flow around a sphere [e.g., *Kundu and Cohen*, 2008, p. 206] reproduces the observed deviation from a logarithmic profile (dashed lines Figure 6). The logarithmic vertical structure of the dominant EOF is consistent with the open-channel flow profile (12) with $\Pi=0$, presumably because the current profiles do not include the upper 20% of the water column where Cole's wake function causes a significant deviation from a log profile [e.g., *Guo and Julien*, 2008].

4.3. Momentum Balance Over the Reef Flat

Focusing on the reef flat, terms in the cross-reef momentum balance are estimated by integrating (5) from SGN to SGS (Figures 2 and 3) and evaluating the resulting terms (6). To estimate the wave-radiation stress gradient, spatial variations in wave height are determined using a wave-transformation model based on a wave-energy balance with a wave-breaking dissipation parameterization proposed by *Thornton and Guza* [1983] and a wave friction factor parameterization proposed by *Soulsby* [1997] [see *Lentz et al*., 2016, for details]. This wave-transformation model accurately reproduces observed wave heights across QD2 [*Lentz et al*., 2016]. The model wave heights are used in (3) to estimate the cross-reef variations of the wave-radiation stress at each sample time. Wind stress is assumed to be spatially uniform and is estimated from the buoy or tower meteorological observations using a bulk formula [*Fairall et al*., 2003].

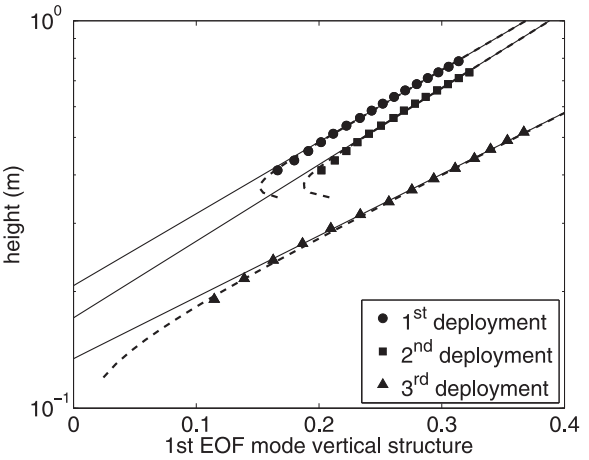

Figure 6. Across-reef current profile structure for largest EOF as a function of log of height above the bottom for the three deployments. Solid lines are log-profile fits to the EOF vertical structure (neglecting the bottom four bins). Dashed lines are estimates of flow distortion due to the current profiler housing assuming potential flow around a sphere with a radius of 0.04 m for the first two deployments when current profiler was mounted on a stand and 0.12 m for the third deployment when it was mounted in a channel attached to the bottom.

The pressure difference $g\Delta\eta$ is estimated directly from the pressure measurements at SGN and SGS. The transport q_o is estimated by integrating the EOF logarithmic profile (Figure 6) extrapolated to the surface and bottom. Cross-reef integrals of D^{-3} and $D^{-1}\partial S_{xx}/\partial x$ are computed at each time step using the water depth $D(x,t)$ determined from the measured bathymetry $h(x)$ (Figure 3) and temporal variations in the average of the sea level variations $\eta_o(t)$ at SGN and SGS (Figure 5d). Finally, the drag coefficient C_{da} is estimated using (13), assuming $\Pi = 0.2$, and choosing a single hydrodynamic roughness $z_o = 0.06$ m for all three deployments that minimized the root-mean-square (RMS) difference between the bottom stress and the sum of the other terms in the momentum balance.

Over the reef flat, the dominant terms in the cross-reef momentum balance are the pressure difference and the integrated bottom stress (Table 1). The nonlinear momentum flux, wave-radiation stress, and wind stress terms are about a factor of 10 smaller than the cross-reef pressure difference. Standard deviations of the residual are a third or less of the standard deviation of the pressure gradient or bottom stress terms, but larger than the other terms. The standard deviations of the residuals correspond to sea level differences of ~3 mm. This suggests the residuals may be due to uncertainties in the pressure measurements, notably inaccurate corrections of drifts and offsets (Appendix B). There is close agreement between the pressure difference term and the integrated bottom stress term (e.g., Figure 7), correlations are ~0.97 for all three deployments and regression coefficients are $0.92-1.04\pm0.07$. The close agreement between the two terms using a single constant z_o supports the assumptions made in deriving the model outlined in section 3 and the estimation of C_{da} given by (14).

To further test the dependence of C_{da} on water depth given by (14), the bulk drag coefficient C_B was estimated in two ways. First, hourly values of C_B were estimated as the ratio of the pressure gradient term and the bottom stress term without C_B, that is (Figure 8, red and blue circles):

$$C_B = -g\Delta\eta / \left(q_o |q_o| \int D^{-3} dx \right). \tag{15}$$

This estimate depends on the measured sea level difference, current profiles, and water depth variations. Second, C_B is estimated directly from (8) and (14) (Figure 8, dashed line). This estimate only depends on $z_o = 0.06$ m and the water depth. The theoretical curve from (8) and (14) reproduces the observed water depth dependence of C_B estimated from the ratio of the momentum balance terms. The bulk drag coefficient C_B is a function of water depth, decreasing rapidly from 0.17 to 0.07 as D/z_o increases from 7 to 12 (D increasing from 0.4 to 0.6 m) and then decreasing more gradually from 0.07 to 0.03 as D/z_o increases from 12 to 20 (D increasing from 0.6 to 1.2 m).

The bottom stress estimates do not include the contribution of the wave-orbital velocities associated with the small surface waves over the reef flat. The ratio of the wave-orbital velocity to the 256 s burst average velocity typically ranges from 0.5 to 2 over the reef flat. The ratio of the estimated pressure gradient term to bottom stress term in (6) shows no significant dependence on the ratio of the wave-orbital velocity to burst-average velocity suggesting that waves do not significantly enhance the bottom stress for the observed conditions over the QD2 reef flat.

4.4. Wave Setup in the Surf Zone

The momentum balance across the surf zone is examined by integrating (5) from RN to SGN and then estimating the terms as described in the previous section. The same hydrodynamic roughness $z_o = 0.06$ m

Table 1. Standard Deviations of Terms in the Cross-Reef Momentum Balance (5) Integrated Across the Reef Flat and Across the Surf Zone for Each Deployment[a]

	Reef Flat—x_{SGN} to x_{SGS}			Surf Zone—x_{RN} to x_{SGN}		
Terms	First Deployment	Second Deployment	Third Deployment	First Deployment	Second Deployment	Third Deployment
$\frac{q_o^2}{D^2}\frac{\partial D}{\partial x}$	0.5	0.5	0.4	0.3	0.2	0.7
$g\frac{\partial \eta}{\partial x}$	8.8	11.4	9.2	10.8	14.3	10.9
$\frac{1}{\rho D}\frac{\partial S_{xx}}{\partial x}$	1.0	0.5		15.5	17.0	18.1
$\frac{\tau^{sx}}{\rho D}$	0.7	0.9	0.5	0.4	0.5	0.3
$\frac{C_{da}q_o\lvert q_o\rvert}{D^3}$	8.4	12.4	9.0	5.1	7.8	4.2
Residual	2.7	3.2	2.9	6.4	8.9	7.1

[a]Units are 10^{-2} ($m^2\ s^{-2}$).

estimated for the reef flat is used in (14). The dominant terms across the surf zone are the pressure difference, the wave-radiation stress convergence and the bottom stress (Table 1). The nonlinear momentum flux and wind stress terms are less than 10% of the pressure difference term. The large bottom stress is in contrast to the traditional wave setup balance on sandy beaches [e.g., *Bowen et al.*, 1968; *Lentz and Raubenheimer*, 1999] where bottom stress is small because of the presence of a coastal boundary and the much smaller bottom drag coefficients.

Incident significant wave heights at RN during events are 0.5–1 m (Figure 5b) and the resulting wave setups are 2–10 cm (e.g., Figure 9). At Abu Madafi, a reef at the shelf edge that is directly exposed to the much larger waves in the Red Sea basin (Appendix A), the observed setup was 35 cm during a 4 m significant wave height event in March 2010. The observed setup at QD2 is highly correlated with the wave-radiation stress convergence (correlations 0.90–0.92) during all three deployments, but the regression slopes are less than 1 $(0.58-0.83\pm0.05)$ (e.g., Figure 9). Including the bottom stress term yields similar correlations (0.92) but regression slopes are closer to 1 $(0.81-1.32\pm0.06)$, indicating the bottom stress partially balances the wave-radiation stress convergence.

The standard deviations of the residuals for the surf zone momentum balance are about 60% of the pressure difference; too large to be attributed entirely to uncertainty in the pressure measurements. A number of factors probably contribute to this discrepancy besides the uncertainty in the pressure difference. The bathymetry at the front edge of the reef is only crudely resolved (Figure 3a) which likely contributes to uncertainty in both the radiation stress and bottom stress terms. The wave-transformation model is another source of uncertainty [*Lentz et al.*, 2016]. The magnitude of the wave-radiation stress term is sensitive to the spatial distribution of the wave-radiation stress relative to the bathymetry. Estimating the wave-radiation stress gradient directly from the observations as a finite difference between RN and SGN yields time series that are highly correlated with the wave-transformation model estimates (correlation 0.98), but with magnitudes that are reduced by 30%–40%. The bottom stress estimate assumes the same hydrodynamic roughness found for the reef flat. This may be an underestimate, as visual inspection suggests the physical roughness is higher at the front edge of the reef than over the reef flat. Also, the bottom stress estimates do not account for surface waves, which should enhance the bottom drag coefficient for the currents [e.g., *Grant and Madsen*, 1982]. While a significant enhancement of bottom stress due to waves was not observed over the reef flat (previous section), in the surf zone wave orbital velocities are almost certainly larger than the mean flow and they may result in larger drag coefficients and bottom stresses.

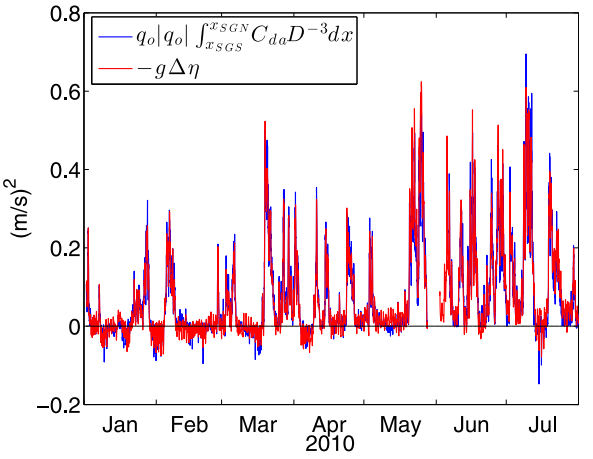

Figure 7. Example of time series of the dominant two terms in the cross-reef momentum balance (6) over the QD2 reef flat—the integrated bottom stress (blue) and the cross-reef pressure difference (red) between SGN and SGS.

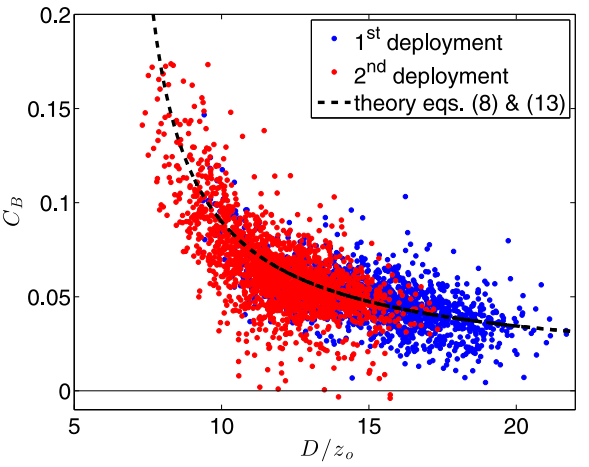

Figure 8. Estimates of the bulk drag coefficient C_B as a function of D/z_o from the ratio of the dominant terms in the cross-reef momentum balance, the pressure difference ($-g\Delta\eta$) and the bottom stress (without C_B; $q_o|q_o|\int_{x_{sgs}}^{x_{sgn}} D^{-3}dx$) for first (blue) and second (red) deployments and theory, equations (8) and (14), (dashed line) which only depends on D, z_o =0.06 m, and $\Pi = 0.2$.

4.5. Evaluation of Model for Currents Over a Platform Reef

Taken together, (9), (11), and (14) comprise a simple analytic model to estimate depth-averaged flow over a flat platform reef, given the hydrodynamic roughness z_o and observations of the incident wave properties, the wind stress, and the water depth. To test the utility of this model, estimates of depth-average cross-reef and along-reef currents determined from (9) and (11) are compared to depth-averaged currents observed over QD2 and two other Red Sea platform reefs, QD1 (Figure 1c) and Al Dagayig (Figure 1b). The incident wave forcing, S_{xx}, at QD1 and QD2 is estimated using data from ADCPs set at S4 and RN, respectively. For Al Dagayig, S_{xx} is estimated using data from a Seagauge pressure sensor deployed in front of the reef (Appendix A). Assuming the major (cross-reef) axis of the subtidal reef currents is aligned with the orientation of the wave forcing, variations in the wave direction are not considered. Wind stress is estimated from the offshore meteorological buoy observations. The drag coefficient C_{da} is estimated from (14) using water depths $D(t)$ obtained from Seagauges deployed on each reef with z_o=0.06 m and Π=0.2 for all three reefs.

Estimates of the cross-reef, depth-averaged flow from (9) are well correlated with the observed depth-average flow, and regression coefficients are 1, except for QD1, indicating the model provides reasonable estimates of the depth-averaged cross-reef flow over these relatively flat platform reefs (Table 2 and Figure 10a). The cross-reef wind stress does not make a significant contribution to the cross-reef currents relative to the wave forcing. The over-estimate of the cross-reef current over QD1 may be due to over-estimating the average water depth because the pressure sensor was in a relatively deep channel compared to the rest of the reef.

Remarkably (11), which assumes the along-reef flow is driven by the along-reef wind stress, has some skill at estimating the observed depth-average along-reef currents (Figure 10b) that are much weaker than the cross-reef currents (Figure 5c). The correlations are lower, and the regression coefficients are more variable, than for the cross-reef flow, particularly at QD1 (Table 2). This indicates that at least a portion of the along-reef flow is wind driven. Variations in the orientation of the surface waves and along-reef topographic variations that are not included in the model probably contribute to the depth-average along-reef currents and hence to the lower correlations.

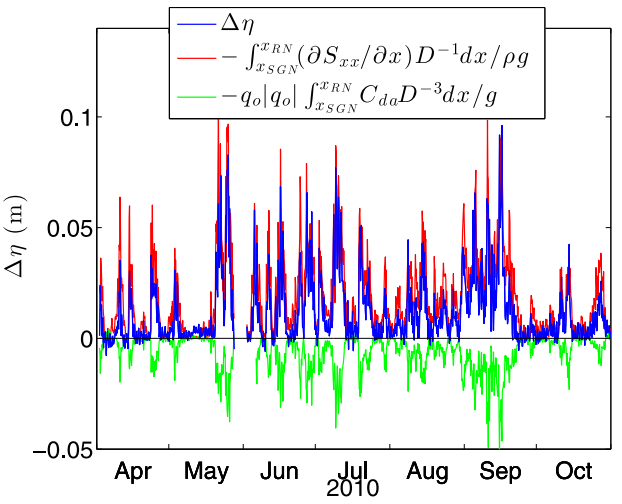

Figure 9. Example of times series of the dominant three terms in the wave setup balance (6) integrated between RN and SGN: setup (blue), wave-radiation stress convergence (red), and bottom stress (green).

5. Discussion

5.1. Drag Coefficients, Hydrodynamic Roughness, and Physical Roughness

The depth-average current drag coefficients for QD2, estimated from (14) with z_o=0.06 m, range from C_{da}=0.13 in 0.4 m water depth to C_{da}=0.03 in 1.2 m water depth. This falls roughly in the middle of the wide range of drag coefficients

Table 2. Results of Linear Regression Analysis Comparing Model Estimates From (9) and (11) and Observed Depth-Averaged Cross-Reef U and Along-Reef V Currents for Three Platform Reefs[a]

		$U_{obs}=aU_{model}+b$			$V_{obs}=aV_{model}+b$			
Site	Δx (m)	corr	a	b (cm s^{-1})	corr	a	b (cm s^{-1})	Days
QD2	200	0.89	1.0 ± 0.03	-5 ± 0.3	0.55	1.4 ± 0.25	1 ± 0.2	320
QD1	230	0.80	0.7 ± 0.02	-1 ± 0.2	0.52	3.9 ± 0.76	2 ± 0.8	363
Al Dagayig	300	0.93	1.0 ± 0.03	-1 ± 0.3	0.56	0.6 ± 0.12	0 ± 0.1	300

[a]Width of reef Δx, length of time series, and 95% confidence intervals for slopes and intercepts are also listed.

reported for coral reefs [e.g., *Rosman and Hench*, 2011]. The estimated hydrodynamic roughness $z_o=0.06$ m is slightly larger than estimates for the Gulf of Aqaba $z_o=0.01$ to 0.04 m [*Reidenbach et al.*, 2006] and much smaller than estimates for Moorea $z_o=0.27$ and 0.41 m [*Rosman and Hench*, 2011]. Physical roughness heights over QD2 range from 0.1 to 0.4 m, with a standard deviation of $\sigma_r=0.13$ m, similar to other coral reef flats [*Reidenbach et al.*, 2006; *Nunes and Pawlak*, 2008; *Péquignet et al.*, 2011; *Jaramillo and Pawlak*, 2011]. The ratio of the hydrodynamic roughness to the standard deviation of the physical roughness is $z_o/\sigma_r \approx 0.5$, which is larger than estimates of this ratio for the Gulf of Aqaba, 0.06–0.25 [*Reidenbach et al.*, 2006]. The QD2 ratio is also large compared to ranges reported for atmospheric boundary layers and laboratory studies [ratios of 0.01–0.4; e.g., *Raupach et al.*, 1991; *Garratt*, 1992; *Britter and Hanna*, 2003; *Jimenez*, 2004].

5.2. Water Depth Dependence of Reef Drag Coefficients

Most previous studies of the momentum balance over coral reefs assume a constant drag coefficient C_{da} for the depth-average current; though see *McDonald et al.* [2006] for a notable exception. Neglect of the dependence of C_{da} on water depth could be misleading when comparing sites on the same reef in different water depths or the same site at different times when there are large temporal changes in water depth. For example, estimates of a constant drag coefficient for the first and second deployments at QD2 are $C_B=0.040\pm0.006$ and $C_B=0.051\pm0.006$, respectively, even though the instrument array and the reef did not change. This difference in the constant C_B between the two deployments is consistent with the water depth being shallower on average during the second deployment relative to the first deployment (Figure 8, compare red and blue circles). The water depth dependence of C_{da} may contribute to the large variations in estimates of reef drag coefficients between different studies [*Rosman and Hench*, 2011].

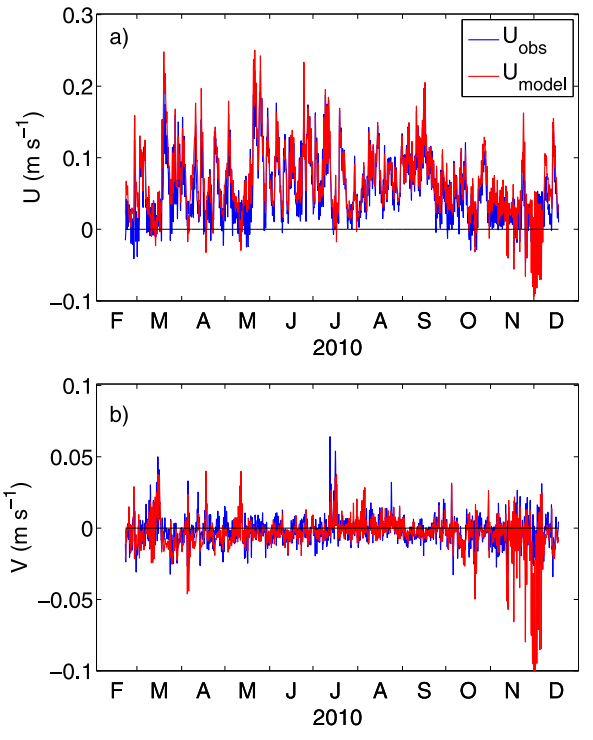

Figure 10. Observed (blue) and modeled (red) (a) cross-reef and (b) along-reef depth-averaged currents over Al Dagayig reef. Modeled currents estimated from incident wave characteristics and wind stress using (9) and (11) as described in section 4.5. Correlations and regression slopes listed in Table 2.

5.3. Surface Wave Dependence of Reef Drag Coefficients

The influence of surface waves on bottom stress and drag coefficients over coral reefs is uncertain [e.g., *Hearn*, 1999; *Reidenbach et al.*, 2006; *Monismith*, 2007; *Rosman and Hench*, 2011]. There are well-developed models characterizing surface gravity wave enhancement of bottom stress and bottom drag coefficients for currents over continental shelves [e.g., *Grant and Madsen*, 1982]. However, some caution is required in applying these models to coral reefs because the models assume the hydrodynamic roughness is small compared to the wave

boundary layer thickness; an assumption that is not valid over many coral reefs. Furthermore, estimated drag coefficients over the QD2 reef flat did not exhibit any dependence on wave orbital velocities divided by the reef current (section 4.3). *Monismith et al*. [2013] also observed that estimated drag coefficients over the Moorea forereef did not depend on the wave height. Clearly, more observations are needed to begin developing a quantitative understanding of how surface waves influence drag over coral reefs.

5.4. Accurate Estimation of Momentum Balance Terms

In section 3.1 (equation (6)) and the subsequent analysis, the cross-reef momentum balance is integrated between pressure measurement sites rather than using a finite difference approximation to estimate the pressure gradient, as in most previous studies. For a flat reef, where the water depth does not vary across the reef, the two approaches are equivalent. However, if there is a cross-reef variation in water depth, the pressure gradient is not constant and a finite difference may give an inaccurate estimate of the magnitude of the pressure gradient. This is evident from (5) which over the reef flat reduces to a balance between the pressure gradient and bottom stress

$$g\frac{\partial \eta}{\partial x} = -C_{da}\frac{q_o|q_o|}{D^3}. \tag{16}$$

The sea surface slope is clearly a strong function of the water depth D because in shallow water the depth-average flow is relatively strong compared to deeper water, consequently the pressure gradient must be larger in shallow water relative to deep water to balance the larger bottom stress. Furthermore, from (14) the drag coefficient is larger in shallow water than in deep water. For example, for a reef that is 200 m wide with the water depth increasing linearly from 1 m at the front edge to 3 m at the back edge, a finite difference using the average water depth (2 m) underestimates the spatial-average pressure gradient by 50%. As a consequence, finite difference estimates of terms in the cross-reef momentum balance will yield inaccurate estimates of the hydrodynamic roughness or the drag coefficient.

5.4. Local Log-Profile Stress Estimates

The logarithmic current profiles in Figure 6 can be used to estimate the local bottom stress by fitting for u_* and z_o [e.g., *Davis and Monismith*, 2011; *Monismith et al*., 2013]. Log-profile estimates of bottom stress, using the EOF analysis in section 4.2, are highly correlated with the cross-reef pressure gradient, but twice the magnitude, and the roughness estimates $z_o \approx 0.15-0.20$ m (Figure 8) are about 3 times larger than the reef flat momentum balance estimates, $z_o = 0.06$ m. Fitting individual profiles to (12) with $\Pi = 0.2$ yields similar results. While one does not expect a local estimate to match the average bottom stress or roughness scale across the reef, the discrepancy seems large. *Rosman and Hench* [2011] observed a similar large discrepancy comparing log-profile and momentum balance estimates of drag coefficients. One issue in this study is that the QD2 current profiles do not include the lower 20% of the water column where vertical variations in the log profile are large [*Guo and Julien*, 2008]. However, a more likely cause for the discrepancy is that the log-profile estimates are sensitive to defining the location of the bottom [e.g., *Raupach et al*., 1991]. The current profiler at AQ1 was in a 2 m wide sand channel that was 0.2–0.4 m deeper than the surrounding reef. The current profiler at AQ2 was in a small sand patch about 0.1 m deeper than the surrounding reef. Log-profile estimates of bottom stress and roughness scales using the EOF analysis (section 4.2) were recomputed adjusting the current profiler bin heights to the effective bottom, $u(z) = \frac{u_*}{\kappa}\log\left(\frac{z-d}{z_o}\right)$, with $d = 0.2$ m at AQ1 and $d = 0.1$ m at AQ2. The resulting roughness scale estimates, $z_o =$ 0.08, 0.06, 0.07 m for the three deployments, and the bottom stresses are more consistent with the reef flat momentum balance estimates (regression slopes between the pressure gradient and log-profile stress estimates are 0.6 to 1.6 ± 0.2).

6. Summary

Analysis of current, pressure, and surface wave observations indicate that cross-reef currents are primarily wave-driven over three platform reefs in the Red Sea. The platform reefs examined are 200–300 m wide and 500 m to several km long (Figures 1 and 2). Water depths on top of the reefs are ~1 m with substantial temporal (Figure 5d) and spatial (Figure 3) variations. At the edge of the reefs, water depths increase abruptly to 10–20 m (Figure 3).

Momentum flux convergence due to waves breaking at the front edge of QD2 reef (wave-radiation stress gradient) causes a sea level setup of 2–10 cm for incident wave heights of 0.5–1 m (Figure 9). Bottom stress is a significant component of the setup balance over QD2 (Figure 9), and presumably over other Red Sea platform reefs, in contrast to sandy beaches where bottom stress is typically not a significant component of the setup balance. The wave-driven setup at the front edge of the reef causes a substantial pressure gradient across the reef since the sea level height at the back edge of the reef is roughly the same as in front of the reef (seaward of the surf zone). The resulting cross-reef current is strong enough that bottom stress balances the cross-reef pressure gradient (Figure 7). The resulting wave-driven cross-reef flows are typically 5–20 cm s^{-1} (Figure 5c) with a logarithmic velocity profile (Figure 6).

An analytical one-dimensional model for the depth-average flow over a flat platform reef is proposed that only depends on the incident wave characteristics, the wind stress, the water depth, the reef width, and the hydrodynamic roughness. Using the single hydrodynamic roughness (z_o=0.06 m) estimated from the QD2 momentum balance and no other adjustable parameters, the model accurately reproduces the observed depth-averaged cross-reef currents over QD2 and two other platform reefs in the Red Sea (Figure 10a and Table 2) and indicates the depth-average cross-reef currents are driven by surface waves. The model also indicates that the much weaker depth-average along-reef currents are partially wind-driven (Figure 10b and Table 2).

A key result of this study is that the drag coefficient, C_{da}, for the depth-averaged current depends on both water depth and hydrodynamic roughness. C_{da} decreases as water depth increases and the dependence is consistent with open-channel flow theory (14) (Figure 8). The estimated hydrodynamic roughness for QD2 from the cross-reef momentum balance is z_o=0.06 m. Uncertainty in drag coefficients and the associated bottom stresses is probably the biggest challenge in accurately modeling currents over coral reefs [*Rosman and Hench*, 2011]. The results presented here highlight three key questions: to what extent are the large variations in reported drag coefficients over coral reefs due to variations in water depth; how do surface gravity waves impact drag coefficients and bottom stress over coral reefs; and what is the relationship between hydrodynamic roughness and physical roughness over coral reefs.

Appendix A: Measurements on Other Reefs

QD1 is an elliptic shaped platform reef in the Qita Dukais reef system that is about 170 m wide and 480 m long (Figure 1c). An Aquadopp current profiler in pulse-coherent mode was deployed in roughly the middle of the reef for two consecutive 6 month periods from 18 October 2008 to 31 October 2009. High-quality current measurements were limited to the lowest four bins from 0.44 to 0.74 mab. An RDI ADCP deployed 800 m south of QD1 (Figure 1c, site S4) provided wave data using the same sampling scheme as the ADCP at RN.

Al Dagayig is a larger, more elongated reef (300 m wide and 1400 m long), located about 30 km northeast of Qita Dukais (Figure 1b). An Aquadopp current profiler, sampling currents in nine 0.05 m bins extending from 0.34 to 0.74 mab, was deployed toward the back of the reef for over a year (6 February 2010 to 16 February 2011). A Seagauge pressure sensor, deployed in 9 m of water about 120 m in front of Al Dagayig, collected wave-bursts at 4 Hz for 1024 s every 2 h to characterize the incident waves.

Abu Madafi is a 300 m wide and 7 km long platform reef located at the outer edge of the continental shelf. Two Seagauges, recording 20 min average pressures, were deployed from April to early November 2009; one on the front edge of Abu Madafi in 0.8 m of water and the other 140 m in front of the reef in 18 m of water. The Seagauge in front of the reef collected wave-bursts at 4 Hz for 512 s every 2 h.

Appendix B: Data Quality and Processing

Bathymetry data over the QD2 reef were collected using a downward-looking Aquadopp mounted on a float sampling 2 cm bins at 1 Hz with a maximum range of about 3 m. The 4° acoustic beams have a footprint diameter of about 8 cm in 1.2 m of water. Water depth was estimated as the depth of the maxima of the near-bottom acoustic backscatter from each beam. A parabola was fit to the acoustic backscatter to more precisely determine the location of the maxima [*Visbeck and Fischer*, 1995; *Shcherbina et al*., 2005]. Estimates of bottom location have an accuracy of about 1 cm based on comparisons between upward looking

Aquadopp estimates of sea level height and Seagauge pressure measurements. The Garmin GPS, sampling at 1 Hz with a position resolution of 10^{-3} min (~2 m), was interpolated to provide higher resolution positions. The float drifted across the reef at about 0.2 m s^{-1}, which given the 1 Hz sample rate, implies a horizontal resolution of about 0.2 m. Bathymetry data was not collected near the front edge of the reef ($0 < x < 40$ m Figure 3a) using the Aquadopp because of breaking waves. Subsequently depth measurements were collected with a cross-reef resolution of about 10 m using a tape measure and handheld GPS during a period when waves were small. Bathymetry from the surrounding shelf (Figure 3b) is from a depth recorder on a small boat.

Processing of the Seagauge pressure time series included eliminating drifts and shifts in the pressure time series due to both the instrument and settling of the instrument platform. The SGN pressure time series was used as a reference because it was firmly attached to the reef and comparison to atmospheric pressure predeployment and postdeployment indicated no instrument drift. Drifts and shifts were determined subjectively by comparing the other pressure time series to the SGN pressure time series. Total estimated drifts over each deployment were typically less than 1 cm, except for the RN and RS tripods deployed on sand bottoms that both settled about 8 cm.

Sea level variations at each site were estimated using the vertically integrated hydrostatic balance:

$$\eta = (P_B - P_A)/g\rho_{DA} - h, \tag{B1}$$

and time series of bottom pressure P_B from the Seagauges, depth-average density ρ_{DA} estimated from temperature/conductivity or temperature measurements, atmospheric pressure P_A from the meteorological buoy and the water depth h relative to mean sea level. To level the sea surface estimates relative to each other, the mean sea level for all times when the current speed is less than 1 cm s^{-1} is set to zero at each site. At RS and over the reef flat, density was estimated from temperature using a linear relationship determined from the RN temperature and density time series, $\rho \approx 1033.2 - 0.28T$, where T is water temperature (°C) and ρ is density (kg m^{-3}).

Quality control of the Aquadopp velocity profiles involved several steps. In pulse-coherent mode, along-beam water speeds are determined by the rate of change in phase between two pulses [e.g., *Zedel et al.*, 1996]. Consequently, speed ambiguity occurs if the phase changes by more than 180°, i.e., wraps. Wrapping was corrected by transforming to beam coordinates and then removing large bin-to-bin velocity jumps associated with phase changes of more than 180°. Wrapping typically occurred in 1% or less of the data. After unwrapping, velocity samples with pulse-to-pulse (beam) correlations less than 20% were discarded because standard deviations of beam speeds were independent of pulse-to-pulse correlations for correlations above 20%, but increased rapidly as correlations decreased below 20%. Depending on the sampling period and bin height, 3–9% of the samples had correlations less than 20%. Bursts with fewer than 50 good velocity samples were discarded. Finally, burst-averaged velocities from bins that were within 15% (20% during the second deployment) of the current profiler depth below the surface were discarded because acoustic side-lobe reflections from the surface contaminate the velocity estimates.

Acknowledgments

The authors are grateful for the scientific and technical support provided by colleagues at King Abdullah University of Sciences and Technology (KAUST), in particular Yasser Abualnaja, Abdulaziz Al-Suwailem, Haitham Aljahdali, Mohsen Aljahdali, Ramzi Aljahdali, Wael Almoazen, Captain Evangelos G. Aravantinos, Yasser Kattan, and all the crew members of the Boston Whaler used in our field work. We also thank C. Marquette, J. Kemp, J. Ryder, S. Whelan, J. Smith, P. Bouchard, J. Lord and the rigging shop, all of Woods Hole Oceanographic Institution, for their efforts in instrument preparation, deployment, and recovery. This research is based on work supported by awards USA 00002 and KSA 00011 KAUST. K. Davis was supported by a WHOI Postdoctoral Fellowship. T. Farrar was partly supported by NSF grant OCE-1435665. S. Lentz was partly supported by NSF grants OCE-1332646 and OCE-1357290. Data are available from the corresponding author (slentz@whoi.edu) upon request, subject to approval from KAUST. The authors thank two anonymous reviewers for comments and suggestions that improved the manuscript.

References

Abdelrahman, S. M. (1997), Seasonal fluctuations of mean sea level at Gizan, Red Sea, *J. Coastal Res.*, *13*, 1166–1172.

Baird, M. E., M. Roughan, R. W. Brander, J. H. Middleton, and G. J. Nippard (2004), Mass-transfer-limited nitrate uptake on a coral reef flat, Warraber Island, Torres Strait, Australia, *Coral Reefs*, *20*, 386–396.

Bowen, A. J., D. L. Inman, and V. P. Simmons (1968), Wave 'set-down' and set-up, *J. Geophys. Res.*, *73*, 2569–2577.

Britter, R. E., and S. R. Hanna (2003), Flow and dispersion in urban areas, *Annu. Rev. Fluid Mech.*, *35*, 469–496.

Callaghan, D. P., P. Nielsen, N. Cartwright, M. R. Gourlay, and T. E. Baldock (2006), Atoll lagoon flushing forced by waves, *Coastal Eng.*, *53*, 691–704, doi:10.1016/j.coastaleng.2006.02.006.

Coronado, C., J. Candela, R. Iglesias-Prieto, J. Sheinbaum, M. Lopez, and F. J. Ocampo-Torres (2007), On the circulation in the Puerto Morelos fringing reef lagoon, *Coral Reefs*, *26*, 149–163, doi:10.1007/s00338-006-0175-9.

Cuet, P., C. Pierret, E. Coridier, and M. J. Atkinson (2011), Water velocity dependence of phosphate uptake on a coral dominated fringing reef flat, La Reunion Island, Indian Ocean, *Coral Reefs*, *30*, 37–43, doi:10.1007/s00338-010-0712-4.

Davis, K. A., and S. G. Monismith (2011), The modification of bottom boundary layer turbulence and mixing by internal waves shoaling on a barrier reef, *J. Phys. Oceanogr.*, *41*, 2223–2241.

Davis, K. A., S. J. Lentz, J. Pineda, J. T. Farrar, V. R. Starczak, and J. H. Churchill (2011), Observations of the thermal environment on Red Sea platform reefs: A heat budget analysis, *Coral Reefs*, *30*, 25–36, doi:10.1007/s00338-011-0740-8.

Fairall, C. W., E. F. Bradley, J. E. Hare, A. A. Grachev, and J. B. Edson (2003), Bulk parameterization of air-sea fluxes: Updates and verification for the COARE Algorithm, *J. Clim.*, *16*, 571–591.

Falter, J. L., M. J. Atkinson, and M. A. Merrifield (2004), Mass-transfer limitation of nutrient uptake by a wave-dominated reef flat community, *Limnol. Oceanogr.*, *49*, 1820–1831.
Garratt, J. R. (1992), *The Atmospheric Boundary Layer*, 316 pp., Cambridge Univ. Press, N. Y.
Gourlay, M. R. (1996a), Wave set-up on coral reefs. 1. Set-up and wave-generated flow on an idealized two dimensional reef, *J. Coastal Eng.*, *27*, 161–193.
Gourlay, M. R. (1996b), Wave set-up on coral reefs. 2. Wave set-up on reefs with various profiles, *J. Coastal Eng.*, *28*, 17–55.
Gourlay, M. R., and G. Colleter (2005), Wave-generated flow on coral reefs: An analysis for two-dimensional horizontal reef-tops with steep faces, *J. Coastal Eng.*, *52*, 353–387.
Grant, W. D., and O. S. Madsen (1982), Movable bed roughness in unsteady oscillatory flow, *J. Geophys. Res.*, *87*, 469–481.
Guo, J., and P. Y. Julien (2008), Application of the modified log-wake law in open-channels, *J. Appl. Fluid Mech.*, *1*(2), 17–23.
Hearn, C. J. (1999), Wave-breaking hydrodynamics within coral reef systems and the effect of changing relative sea level, *J. Geophys. Res.*, *104*, 30,007–30,019, doi:10.1029/1999JC900262.
Hearn, C. J. (2010), Hydrodynamics of coral reefs, in *Encyclopedia of Modern Coral Reefs*, edited by D. Hopley, pp. 563–573, Springer, Berlin.
Hearn, C. J. (2011), Perspectives in coral reef hydrodynamics, *Coral Reefs*, *30*, 1–9, doi:10.1007/s00338-011-0752-4.
Hench, J. L., J. J. Leichter, and S. G. Monismith (2008), Episodic circulation and exchange in a wave-driven coral reef and lagoon system, *Limnol. Oceanogr.*, *53*(6), 2681–2694, doi:10.4319/lo.2008.53.6.2681.
Jago, O. K., P. S. Kench, and R. W. Brander (2007), Field observations of wave-driven water-level gradients across a coral reef flat, *J. Geophys. Res.*, *112*, C06027, doi:10.1029/2006JC003740.
Jaramillo, S., and G. Pawlak (2011), AUV-based bed roughness mapping over a tropical reef, *Coral Reefs*, *30*, 11–23, doi:10.1007/s00338-011-0731-9.
Jiang, H., J. T. Farrar, R. C. Beardsley, R. Chen, and C. Chen (2009), Zonal surface wind jets across the Red Sea due to mountain gap forcing along both sides of the Red Sea, *Geophys. Res. Lett.*, *36*, L19605, doi:10.1029/2009GL040008.
Jimenez, J. (2004), Turbulent flows over rough walls, *Annu. Rev. Fluid Mech.*, *36*, 173–196.
Kraines, S. B., T. Yanagi, M. Isobi, and H. Komiyama (1998), Wind-wave driven circulations on the coral reef at Bora Bay, Miyako Island, *Coral Reefs*, *17*, 133–143, doi:10.1007/s003380050107.
Kundu, P. K., and I. M. Cohen (2008), *Fluid Mechanics*, 872 pp., Elsevier, Burlington, Mass.
Lentz, S., and B. Raubenheimer (1999), Field observations of wave setup, *J. Geophys. Res.*, *104*, 25,867–25,875, doi:10.1029/1999JC900239.
Lentz, S., R. T. Guza, S. Elgar, F. Feddersen, and T. H. C. Herbers (1999), Momentum balances on the North Carolina inner shelf, *J. Geophys. Res.*, *104*, 18,205−18,226.
Lentz, S. J., J. H. Churchill, K. A. Davis, and J. T. Farrar (2016), Surface gravity wave transformation across a platform coral reef in the Red Sea, *J. Geophys. Res. Oceans*, *121*, doi:10.1002/2015JC011142, in press.
Longuet-Higgins, M. S., and R. W. Stewart (1962), Radiation stresses in water waves: A physical discussion, with applications, *Deep Sea Res. Oceanogr. Abstr.*, *11*, 529–562.
Longuet-Higgins, M. S., and R. W. Stewart (1964), Radiation stresses and mass transport in gravity waves, with application to "surf-beats," *J. Fluid Mech.*, *13*, 481–504.
Lowe, R. J., J. L. Falter, S. G. Monismith, and M. J. Atkinson (2009), Wave-driven circulation of a coastal reef–lagoon system, *J. Phys. Oceanogr.*, *39*(4), 873–893, doi:10.1175/2008JPO3958.1.
Manasrah, R., H. M. Hasanean, and S. Al-Rousan (2009), Spatial and seasonal variations of sea level in the Red Sea, 1958–2001, *Ocean Sci. J.*, *44*, 145–159.
Massel, S. R., and M. R. Gourlay (2000), On the modeling of wave breaking and set-up on coral reefs, *J. Coastal Eng.*, *39*, 1–27.
McDonald, C. B., J. R. Koseff, and S. G. Monismith (2006), Effects of the depth to coral height ratio on drag coefficients for unidirectional flow over coral, *Limnol. Oceanogr.*, *51*(3), 1294–1301.
Mei, C. C. (1983), *The Applied Dynamics of Ocean Surface Waves*, 740 pp., John Wiley, N. Y.
Monismith, S. G. (2007), Hydrodynamics of coral reefs, *Annu. Rev. Fluid Mech.*, *39*, 37–55, doi:10.1146/annurev.fluid.38.050304.092125.
Monismith, S. G., A. Genin, M. A. Reidenbach, G. Yahel, and J. R. Koseff (2006), Thermally driven exchanges between a coral reef and the adjoining ocean, *J. Phys. Oceanogr.*, *36*, 1332–1347.
Monismith, S. G., L. M. M. Herdman, S. Ahmerkamp, and J. L. Hench (2013), Wave transformation and wave-driven flow across a steep coral reef, *J. Phys. Oceanogr.*, *43*, 1356–1379.
Morcos, S. A. (1970), Physical and chemical oceanography of the Red Sea, *Oceanogr. Mar. Biol. Ann. Rev.*, *8*, 73–202.
Munk, W. H., and M. C. Sargent (1948), Adjustment of Bikini atoll to ocean waves, *Trans. AGU*, *29*, 855–860.
Nelson, R. C. (1996), Hydraulic roughness of coral reef platforms, *Appl. Ocean Res.*, *18*, 265–274.
Nezu, I., and H. Nakagawa (1993), *Turbulence in Open-Channel Flows*, 281 pp., A. A. Balkema, Rotterdam, Netherlands.
Nunes, V., and G. Pawlak (2008), Observations of bed roughness of a coral reef, *J. Coastal Res.*, *24*, 39–50, doi:10.2112/05-0616.1.
Oliver, T. A., and S. R. Palumbi (2011), Do fluctuating temperature environments elevate coral thermal tolerance?, *Coral Reefs*, *30*, 241–250, doi:10.1007/s00338-011-0721-y.
Osman, M. M. (1985), Seasonal and secular variations of sea level at Port Sudan, *J. Fac. Mar. Sci.*, *4*, 15–25.
Péquignet, A.-C., J. M. Becker, M. A. Merrifield, and S. J. Boc (2011), The dissipation of wind wave energy across a fringing reef at Ipan, Guam, *Coral Reefs*, *30*, 71–82, doi:10.1007/s00338-011-0719-5.
Pineda, J., V. Starczak, A. M. Tarrant, J. Blythe, K. A. Davis, T. Farrar, M. L. Berumen, and J. C. B. Da Silva (2013), Two spatial scales in a bleaching event: Corals from the mildest and the most extreme thermal environments escape mortality, *Limnol. Oceanogr.*, *58*, 1531–1545, doi:10.4319/lo.2013.58.5.1531.
Raupach, M. R., R. A. Antonia, and S. Rajagopalan (1991), Rough-wall turbulent boundary layers, *Appl. Mech. Rev.*, *44*, 1–25.
Reidenbach, M. A., S. G. Monismith, J. R. Koseff, G. Yahel, and A. Genin (2006), Boundary layer turbulence and flow structure over a fringing coral reef, *Limnol. Oceanogr.*, *51*(5), 1956–1968.
Roberts, H. H., S. P. Murray, and J. H. Suhayda (1975), Physical processes in a fringing reef system, *J. Mar. Res.*, *33*, 233–260.
Rosman, J. H., and J. L. Hench (2011), A framework for understanding drag parameterizations for coral reefs, *J. Geophy. Res.*, *116*, C08025, doi:10.1029/2010JC006892.
Schlichting, H. (1968), *Boundary-Layer Theory*, 747 pp., McGraw-Hill, N. Y.
Shcherbina, A. Y., D. L. Rudnick, and L. D. Talley (2005), Ice-draft profiling from bottom-mounted ADCP, *J. Atmos. Oceanic Technol.*, *22*, 1249–1266.
Sofianos, S. S., and W. E. Johns (2003), An Oceanic General Circulation Model (OGCM) investigation of the Red Sea circulation: 2. Three-dimensional circulation in the Red Sea, *J. Geophy. Res.*, *108*(C3), 3066, doi:10.1029/2001JC001185.

Soulsby, R. L. (1997), *Dynamics of Marine Sands. A Manual for Practical Applications*, Thomas Telford, London, U. K.
Sultan, S. A. R., F. Ahmad, and A. El-Hassan (1995), Seasonal variations of the sea level in the central part of the Red Sea, *Estuarine Coastal Shelf Sci.*, *40*, 1–8.
Symonds, G., K. P. Black, and I. R. Young (1995), Wave-driven flow over shallow reefs, *J. Geophys. Res.*, *100*, 2639–2648, doi:10.1029/94JC02736.
Taebi, S., R. J. Lowe, C. B. Pattiaratchi, G. N. Ivey, G. Symonds, and R. Brinkman (2011), Nearshore circulation in a tropical fringing reef system, *J. Geophys. Res.*, *116*, C02016, doi:10.1029/2010JC006439.
Tait, R. J. (1972), Wave set-up on coral reefs, *J. Geophys. Res.*, *77*, 2207–2211.
Thornton, E. B., and R. T. Guza (1983), Transformation of wave height distribution, *J. Geophys. Res.*, *88*, 5925–5938.
Veron, F. and W. K. Melville (1999), Pulse-to-pulse coherent Doppler measurements of waves and turbulence, *J. Atmos. Oceanic Technol.*, *16*, 1580–1597.
Vetter, O., J. M. Becker, M. A. Merrifield, A.-C. Pequignet, J. Aucan, S. J. Boc, and C. E. Pollock (2010), Wave setup over a Pacific Island fringing reef, *J. Geophys. Res.*, *115*, C12066, doi:10.1029/2010JC006455.
Visbeck, M., and J. Fischer (1995), Sea surface conditions remotely sensed by upward-looking ADCPs, *J. Atmos. Oceanic Technol.*, *12*, 141–149.
Von Arx, W. S. (1954), Circulation systems of Bikini and Rongelap lagoons, Bikini and nearby atolls, Marshall Islands, *U.S. Geol. Surv. Prof. Pap.*, *260-B*, 265–273.
Zedel, L., A. E. Hays, R. Cabrera, and A. Lohrmann (1996), Performance of a single-beam pulse-to-pulse coherent Doppler profiler, *IEEE J. Oceanic Eng.*, *21*, 290–297.